**Author(s):** Tuokko, Sakari; Honkala, Karoliina; Pihko, Petri

**Title:** Pd/C-Catalyzed Hydrosilylation of Enals and Enones with Triethylsilane: Conformer Populations Control the Stereoselectivity

**Year:** 2017

**Version:**

**Please cite the original version:**

Tuokko, S., Honkala, K., & Pihko, P. (2017). Pd/C-Catalyzed Hydrosilylation of Enals and Enones with Triethylsilane: Conformer Populations Control the Stereoselectivity. ACS Catalysis, 7(1), 480-493. https://doi.org/10.1021/acscatal.6b02856

# Pd/C Catalyzed Hydrosilylation of Enals and Enones with Triethylsilane: Conformer Populations Control the Stereoselectivity

*Sakari Tuokko, Karoliina Honkala* and Petri M. Pihko*[*]

AUTHOR ADDRESS Department of Chemistry, Nanoscience Center, University of Jyväskylä, P.O. Box 35, 40014, Jyväskylä (Finland) E-mail:petri.pihko@jyu.fi, karoliina.honkala@jyu.fi

ABSTRACT: The palladium-on-charcoal catalyzed chemo-, regio-, and stereoselective 1,4-hydrosilylation and transfer hydrogenation reactions of α,β-unsaturated aldehydes and ketones with triethylsilane have been investigated with a combination of experimental and theoretical methods . The reaction mechanism has been studied experimentally by monitoring the reactions by $^{1}$H NMR from aliquots withdrawn from the stirred reaction mixtures, labeling experiments, and control experiments. Our density functional theory results indicate that both above mentioned reactions initiate with a dissociative adsorption of the triethylsilane on the palladium catalyst. In the hydrosilylation reaction, the α,β-unsaturated aldehyde or cyclic ketone is adsorbed on the silyl-covered palladium catalyst , where it is first irreversibly *O*-silylated and then reduced by a hydride addition to the 4-position. The *O*-silylation step has a low barrier, and it essentially freezes the solution-phase *s*-trans:*s*-cis conformer ratio in the form of enol silane stereoisomers. In support of

the stereoselectivity model, the experimental *Z*:*E* stereoselectivities of enol silane products are in very close agreement with the computed *s*-trans:*s*-cis conformer population ratios. The transfer hydrogenation reaction is carried out in the presence of water, and there the product is a saturated aldehyde or ketone. In this reaction regime, the silyl species on the palladium surface rapidly reacts with water to give triethylsilanol as a side product. The α,β-unsaturated carbonyl is then adsorbed on the palladium surface, where it undergoes a conjugate reduction in a 1,4-fashion: the hydride addition to the 4-position occurs on the palladium surface, giving an enolate-type intermediate which is then protonated by the protic solution phase. Finally, we present a revised protocol for the stereoselective hydrosilylation reaction with Pd/C that improves the product stereoselectivity by a proper choice of solvent and reaction time.

KEYWORDS Heterogeneous, catalysis, Pd/C, DFT, reaction mechanism, chemoselective, stereoselective, hydrosilylation, transfer hydrogenation.

## INTRODUCTION

Among the reactions catalyzed by the supported catalysts, the truly heterogeneous surface reactions usually comprise direct hydrogenations or oxidations.[1] A significant challenge for heterogeneous catalysis is to control the chemo- and regioselectivity or potentially stereo– and enantioselectivity.[2] In spite of the operational simplicity of typical reactions carried out on supported metal catalysts, the origins of any observed selectivities have remained largely unknown due the lack of understanding the reaction mechanisms on the metal nanoparticles/colloids.[3] The difficulty to identify reaction intermediates during the catalytic cycle on the supported catalyst makes the mechanistic studies challenging compared to homogenously catalyzed reactions. However, a combination of experimental and theoretical (e.g. DFT) studies can help to distinguish between different intermediates, elementary steps and reaction pathways, and suggest a plausible reaction mechanism for a given transformation.[4,5] Herein, we present the combined experimental and computational study of the mechanism of the Pd/C catalyzed surface reaction of 1,4-hydrosilylation of enals with triethylsilane.[6]

Single enol silane stereoisomers are very valuable compounds in a many stereospecific transformations. For example, the stereochemical outcome of the Mukaiyama regime of aldol and Mannich reactions[7] is dependent on the stereochemistry of the enol silane. Transmetalation of enol silanes to give other metal enolates usually proceeds with high stereochemical fidelity, affording enolate stereoisomers that may not otherwise be accessible.[8] Enol silanes can be obtained via hydrosilylation (conjugate reduction)[9] of the corresponding unsaturated carbonyl compounds, or via direct enolization of ketones in the presence of a silyl halide or silyl pseudohalide (e.g. triflate). However, enolization reactions with aldehydes are experimentally capricious due to a competing nucleophilic attack of the base or self-condensation reactions. The hydrosilylation method usually

displays a preference for (*E*)-enol silanes, and methods to uniformly produce (*Z*)-enol silanes are rare.[10] Catalytic hydrosilylation of α,β-unsaturated aldehydes and ketones with a range of different homogeneous metal catalysts has also been described, including copper,[11] palladium,[12] rhodium,[13] and other metal complexes as catalysts.[14] However, heterogeneous catalysis of the hydrosilylation reaction is an alternative that has been less explored. Other reactions with silyl hydrides on supported metal catalysts, such as Fukuyama reduction of thioesters,[15] or transfer hydrogenations[16] are, however, well established protocols.

## METHODS

**EXPERIMENTAL METHODS.** All reactions were carried out in screw cap glass vials or septum cap glass flasks under air atmosphere, unless otherwise noted. THF, $Et_2O$, DCM, MeCN, and toluene were obtained by passing deoxygenated solvents through activated alumina columns (MBraun SPS-800 Series solvent purification system). Other solvents and reagents were used as obtained from the supplier, unless otherwise noted. Analytical TLC was performed using Merck silica gel F254 (230–400 mesh) plates and analyzed by UV light or by staining upon heating with vanillin solution (6 g of vanillin, 5 mL of conc. $H_2SO_4$, 3 mL of glacial acetic acid, 250 mL of EtOH) or $KMnO_4$ solution (1 g of $KMnO_4$, 6.7 g of $K_2CO_3$, 1.7 mL of 1 M NaOH, 100 mL of $H_2O$). For silica gel chromatography, the flash chromatography technique was used, with Merck silica gel 60 (230–400 mesh) and p.a. grade solvents unless otherwise noted. A small pad of alumina (neutral) columns were prepared by filling plastic syringes (5–20 mL) with Sigma-Aldrich purum p.a. grade alumina. The $^1$H NMR and $^{13}$C NMR spectra were recorded in $CDCl_3$ on Bruker Advance 400 spectrometer. The chemical shifts are reported in ppm relative to residual $CHCl_3$ (δ 7.26) for $^1$H NMR. For the $^{13}$C NMR spectra, the residual $CDCl_3$ (δ 77.16) was used as the internal standards. IR spectra were recorded on a Tensor27 FT-IR spectrometer. High -resolution mass spectrometric data were prepared using MicroMass LCT Premier Spectrometer.

**COMPUTATIONAL METHODS.** Density functional theory (DFT) calculations (exceptions, see below) have been performed with the GPAW code[17,18] which implements the projector augmented wave method (PAW)[19] in a real space grid. Kohn-Sham equations were solved self-consistently using the RPBE[20] GGA (generalized gradient approximation) or van der Waals corrected BEEF-vdW[21] functional to describe exchange and correlation effects. The clean Pd(111) surface was modeled with four-atom-layer-thick slabs with the lattice constant of $a$ = 3.952 Å. The

vacuum in the direction perpendicular to the Pd(111) surface was 6 Å below the bottom metal layer and 10 Å above the top metal layer of the slab. The adsorbate coverage was modeled with (2 x 3), (3 x 3) and (4 x 4) super-cells which corresponds to 1/6 ML (ML = monolayer), 1/9 ML and 1/16 ML coverages, respectively. The Brillouin zone was sampled with 6 x 4 x 1 Monkhorst-Pack *k*-points for the (2 x 3) supercell and 4 x 4 x 1 *k*-points for (3 x 3) and (4 x 4) supercells. The two bottom metal layers were fixed to their ideal bulk positions, while all the other atoms were relaxed until the residual force was below 0.05 eV/Å. The transition states of the elementary reactions were determined using a Nudge Elastic Band (NEB) method or a constrained search (CS) where the interatomic distance of a forming bond is fixed to several values and the remaining degrees of freedom are relaxed. For the found transition states, harmonic frequencies were calculated. Only a single imaginary frequency was obtained for each H-addition, and the visualization of the vibration mode showed bond stretching along a reaction coordinate.

The energies and geometries of the stationary points for s-trans and s-cis conformations of enals in Tables 1 and 2 and for (*E*)- and (*Z*)-isomers of enol silanes **1b** and **2b** were obtained as follows. The initial structures for the geometry optimizations were generated by a 10000 step Monte Carlo conformational search using OPLS2005 force field as implemented in the MacroModel suite of Schrodinger Maestro software.[22a] For each s-trans and s-cis conformers as well as for (Z)- and (E)-isomers of enol silanes **1b** and **2b**, ten lowest non-redundant conformers were further refined by density functional theory (DFT) optimization (M06-2X/6-311G**++)[23] in the Jaguar module[22b] of the Maestro suite and ranked by both gas phase as well as solution phase energies. Only the lowest energy conformers were considered in the population analysis. The error associated with this assumption is predicted to be minor, as evidenced by the results obtained with aldehyde **9a**, where a full population analysis was carried out (see the Supporting Information). The computed s-

trans:s-cis ratio remained unchanged (96:4 in the gas phase, 98.5:1.5 in the solution phase) even when minor conformers were taken into account.

## RESULTS

Our recently published protocol enables to access (*Z*)-enol silanes from α-substituted enals (typically *Z*:*E* > 50:1) and (*E*)-enol silanes from β-substituted enals (typical *Z*:*E* 10:90, Scheme 1a).[6] The chemoselectivity of the hydrosilylation reaction is very high with α-substituted enals, with at most traces of saturated aldehyde is detected as a side-product. With β-substituted enals, saturated aldehydes were typically obtained in 5 – 10 % yields. However, the adding just a small amount of acid to the reaction mixture changes the reaction outcome completely, with the saturated aldehyde as the sole product (Scheme 1b).[6a]

The stereoselectivity of the hydrosilylation reaction is lower with β-substituted enals than with α-substituted enals. In addition, with β-substituted enals, isomerization of the (*E*)- to (*Z*)-enol silane after the completion of the reaction was observed.[6a]

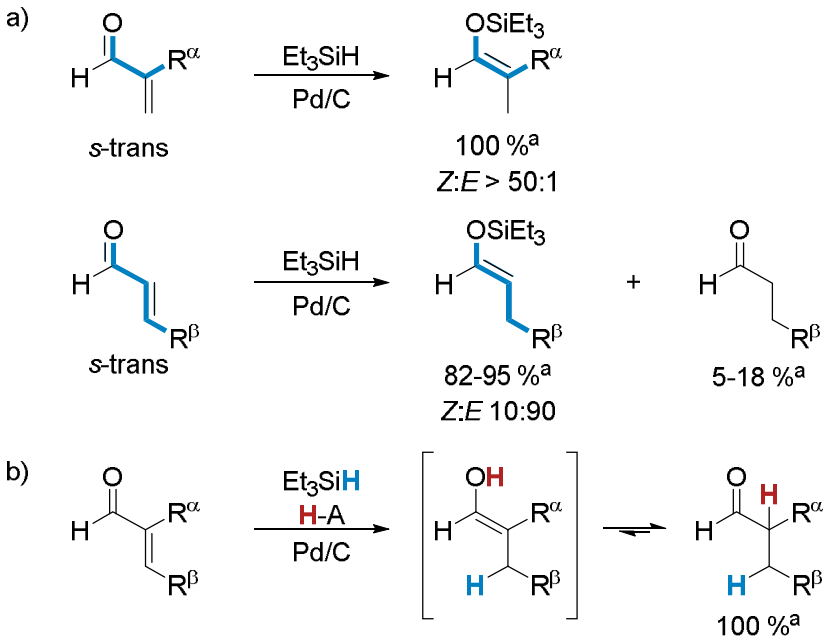


**Scheme 1.** a) Pd/C catalyzed hydrosilylation of α- and β-substituted enals. b) Pd/C catalyzed transfer hydrogenation of enal. [a]Selectivity was determined by $^{1}$H NMR analysis.

In our previous studies, we have established that the nature of the real catalyst is heterogeneous (surface reaction) and not a leached palladium species in the solution.[6b] In addition, crossover experiments with two different silanes demonstrated that silanes such as $Et_3SiH$ are likely to fully dissociate on Pd colloids[24] since the H/D labels and silyl moieties were completely scrambled (Scheme 2a) and $Et_3SiH$ can dissociate on the Pd surface to generate adsorbed hydrogen similarly to $H_2$ dissociation.[25] Labeling experiments have also confirmed that in both hydrosilylation and transfer hydrogenation conditions, $Et_3SiH$ is the source of H-atom adding to the β-position of the enal (Scheme 2b).[6a]

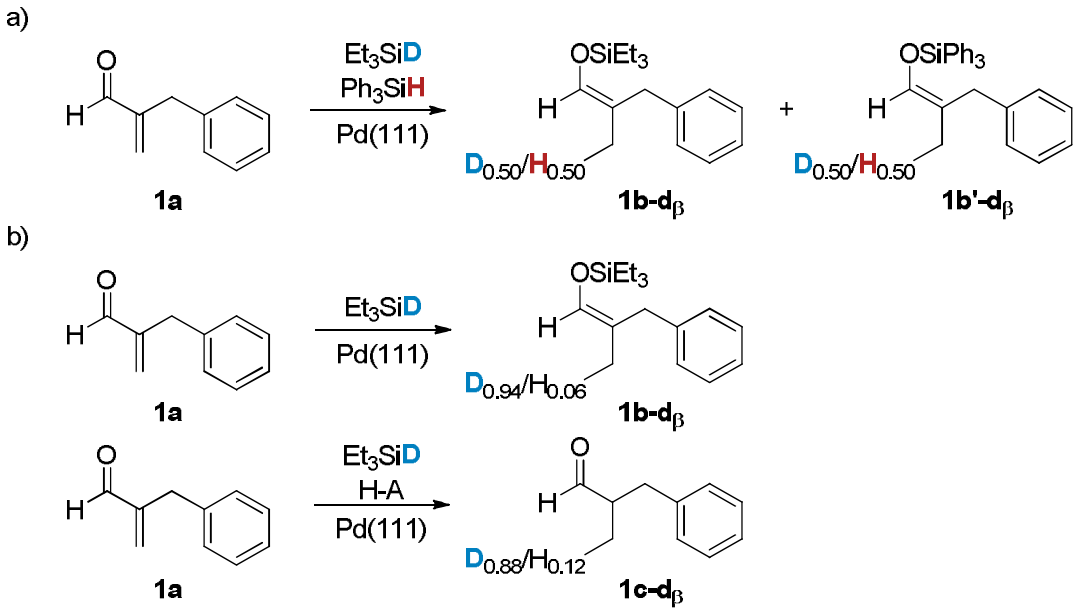


**Scheme 2.** a) Crossover and b) labeling experiments from previous studies.

**REACTION MONITORING EXPERIMENTS.** The issue of the chemoselectivity and the different amount of saturated aldehyde side product observed with α- and β-substituted enals was addressed with NMR monitoring of the reactions. The hydrosilylation and the transfer hydrogenation [with $H_2O$ and $H_2SO_4$ (1 M)] reactions of α-benzyl acrolein (**1a**) and (*E*)-hexenal

(**2a**) were studied.[26] The combined results of the monitoring experiments and relative rates of the reactions are presented in Scheme 3.

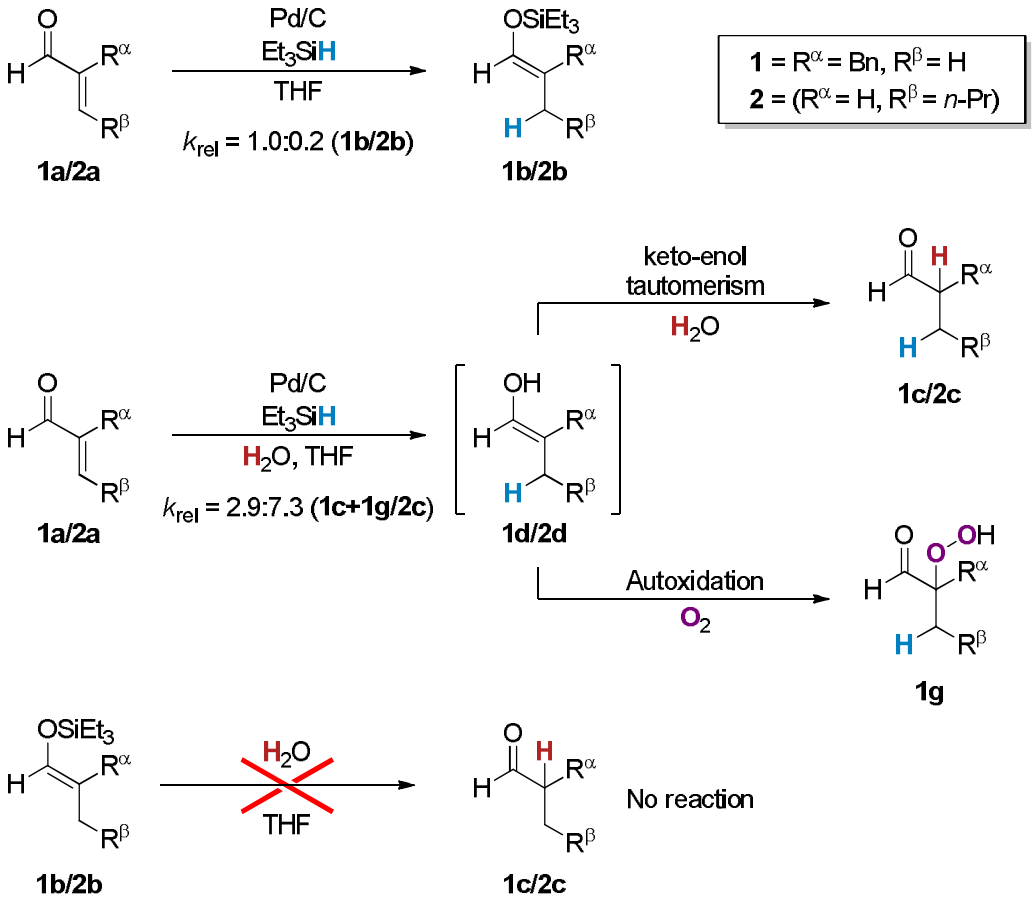


**Scheme 3**. Combined relative rates of hydrosilylation, transfer hydrogenation (in the presence of $H_2O$) and hydrolysis reactions based on reaction monitoring experiments with aliquots withdrawn from the reaction mixtures (see Figure 1). Steady state rates are given after the induction period, see Figure 1. All rates are given relative to the hydrosilylation reaction of α-benzyl acrolein **1a** ($k_{\mathbf{1a}}$ is set to 1.0)

The relative reaction rates clearly illustrate that the saturated aldehyde side product (**1c** and **2c**) formed during the hydrosilylation reaction does not arise from hydrolysis of the corresponding enol silane (**1b** and **2b**), as the enol silanes are stable in the presence of water, even in presence of water and Pd/C i.e. transfer hydrogenation conditions.[27,6b] Importantly, with the α-substituted enal **1a** the rate of the transfer hydrogenation reaction is 3 times faster than the hydrosilylation reaction

(Scheme 3, relative rates 2.9:1.0). However, with the β-substituted enal **2a**, the transfer hydrogenation (with added water) proceeds over 37 times faster than the hydrosilylation (Scheme 3, relative rates 7.3:0.2). We then varied the amount of water in the reaction mixture with enal **2a** (Figure S9). The results indicate that, with 1 equiv. or more of $H_2O$, the formation of **2c** was accelerated (by a factor of 2) compared to "dry" reaction conditions.[28] In addition, with less than 1 equiv. of water, the formation of **2c** appears to slow down during the first minute of the reaction.

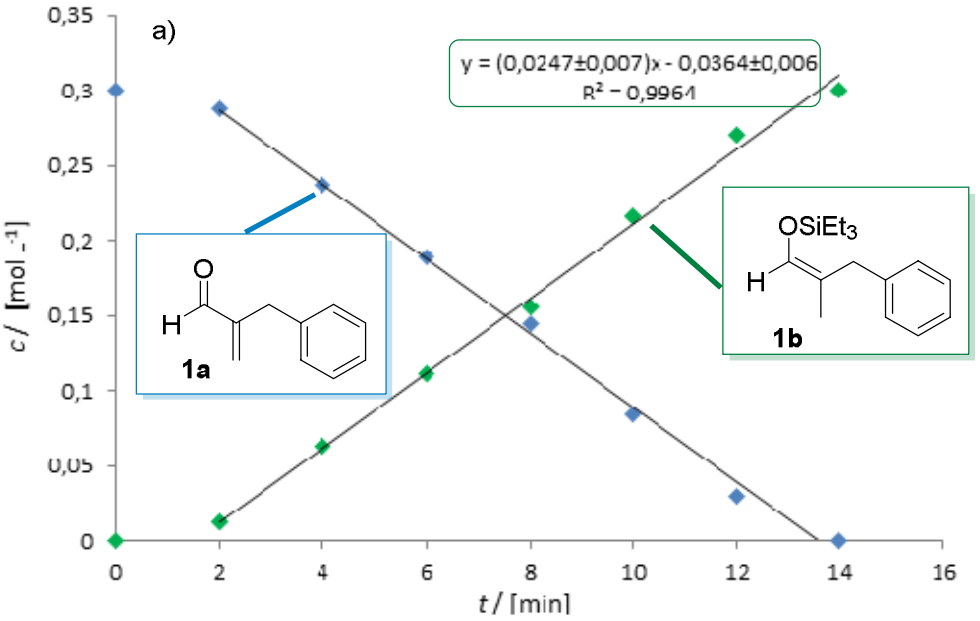
a)
y = (0,0247±0,007)x - 0,0364±0,006
R² = 0,9961
1a
OSiEt3
1b
c / [mol L-1]
t / [min]

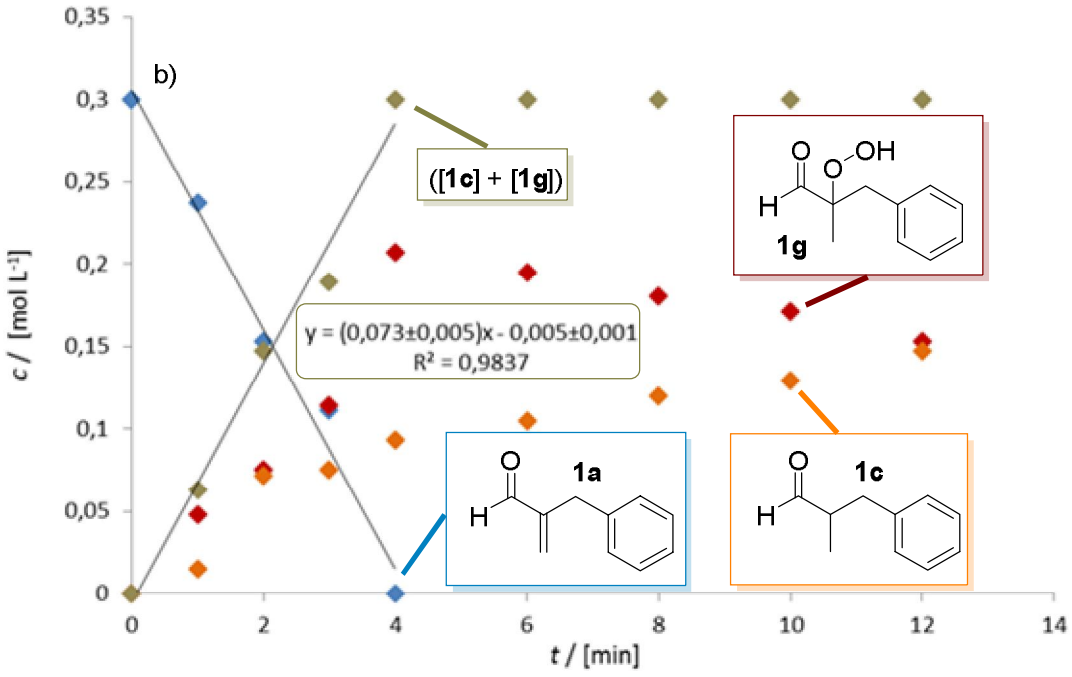
b)
([1c] + [1g])
y = (0,073±0,005)x - 0,005±0,001
R² = 0,9837
1g
1a
1c
c / [mol L-1]
t / [min]

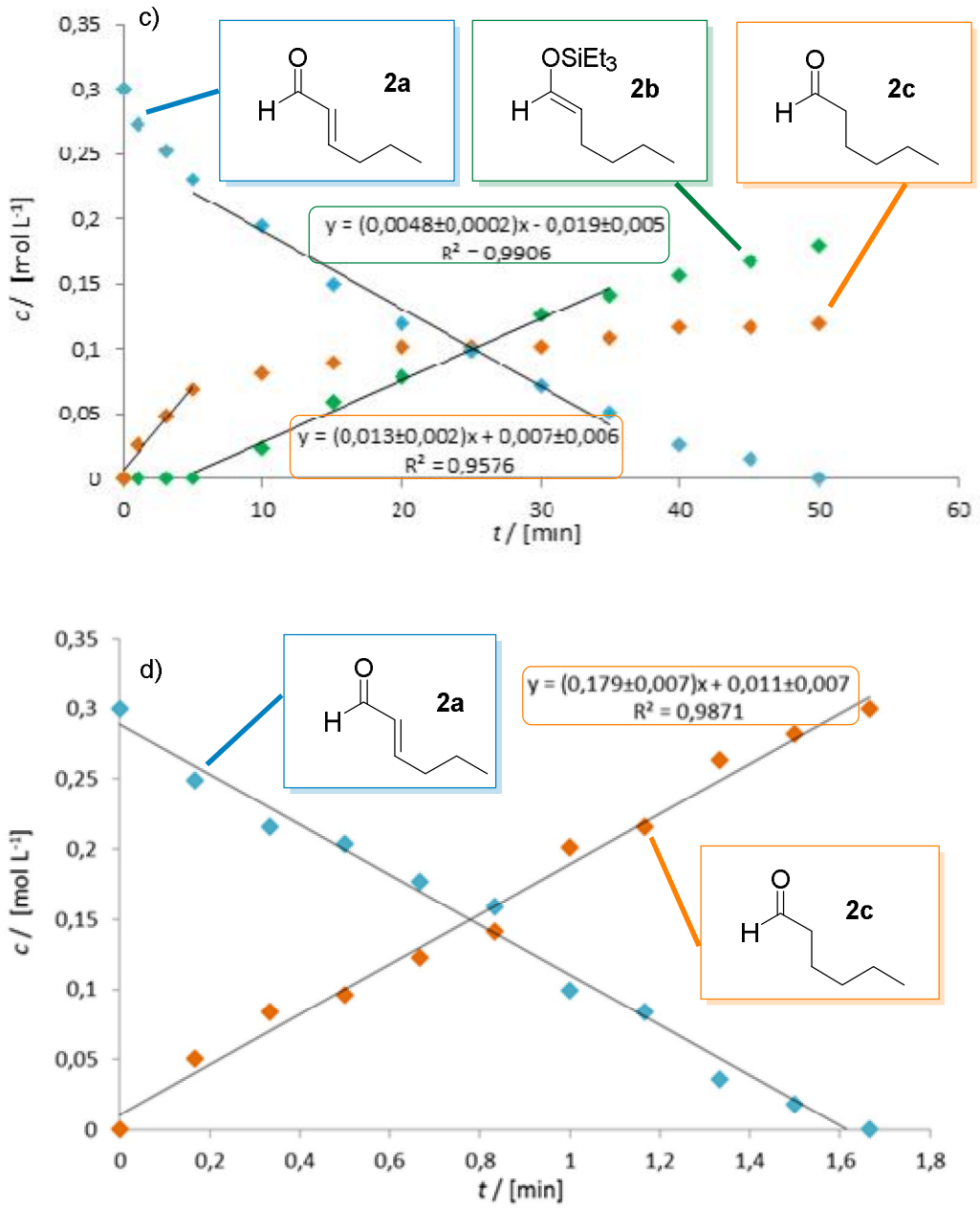


**Figure 1.** Temporal evolution of the hydrosilylation and the transfer hydrogenation reactions: a) hydrosilylation of **1a**, b) transfer hydrogenation (with $H_2O$) of **1a**, c) hydrosilylation of **2a** and d) transfer hydrogenation (with $H_2O$) of **2a**. In all cases, the concentrations of reactants or products were determined by $^1H$ NMR from aliquots withdrawn from the stirred reaction mixtures. For more details, see the Supporting Information.

The more detailed reaction monitoring data (Figure 1) shows that, in both hydrosilylation and transfer hydrogenation conditions, the conversion of **1a** and **2a** appears to follow a "zero-order kinetics" (Figure 1). In the case of hydrosilylation of **2a**, the reaction rate is obtained after initiation period, in which the most of **2c** side product is formed (Figure 1c). Nevertheless, the apparent "zero-order" dependency of the rate from the starting material concentration indicates that, in both hydrosilylation and transfer hydrogenation reactions, the reduction step is mediated by the heterogeneous catalyst which is likely to be saturated with the substrate.

In the transfer hydrogenation conditions with **1a** (Figure 1b), an off-cycle hydroperoxide product **1g** is observed. **1g** is formed via autoxidation of the enol intermediate **1d** when exposed to air,[29] and **1g** can be converted to the corresponding saturated aldehyde **1c** with the addition of acid. In light of our previous studies,[30] **1g** is mainly formed during the sample preparation when the corresponding enol **1d** is exposed to air. As such, the hydroperoxide can be viewed as a proxy for enol intermediate **1d** in Figure 1b. The results in Figure 1b shows that the enol concentration (i.e. hydroperoxide **1g**) builds up and decays in the initial stage of the reaction, and the formation of the aldehyde **1c** appears to follow a sigmoidal curve.[31] This could indicate that the tautomerization of enol **1d** to **1c** occurs in the solution phase instead of being mediated by the heterogeneous catalyst. Additionally, the seemingly linear decay of the starting material **1a** suggest that the initial reduction to enol **1d (**i.e. [**1c**] + [**1g**] in Figure 1b) is mediated by the heterogeneous catalyst, as previously discussed. In the case of enal **2a**, tautomerization to form **2c** is apparently faster than the initial heterogeneous reduction of **2a**, as the formation of the **2c** appears as a linear curve rather that sigmoidal (Figure 1d).

To address the possible mechanism of the saturated aldehyde formation during the hydrogenation of β-substituted enals, we carried out a labeling experiment with $Et_3SiD$ and citral

(**3a**)[32] and isolated the saturated aldehyde side-product **3c** (eq 1). If **3c** is formed by two D-atoms adding to the C=C double bond (3,4-addition), like hydrogenation of the alkenes, we should observe deuterium in both α- and β-position. However, no D-incorporation in the α-position was observed in the $^1$H NMR-measurements.[27] A control experiment with **3c** in the presence of Pd/C, THF and $D_2O$ (rt, 1 h) indicated that background H/D exchange in the α-position is not significant under these conditions.[27] Hence, the saturated aldehyde **3c** is most likely formed via a-protonation of the enol intermediate (i.e. via a transfer hydrogenation pathway).[30]

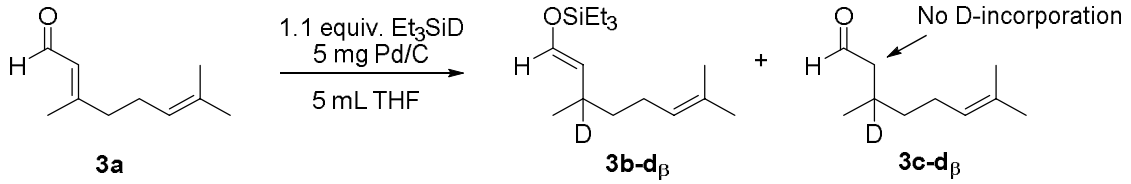


**3a** **3b-d$_\beta$** **3c-d$_\beta$** (1)

Next, we tried to rationalize the difference in stereoselectivity observed with α- and β-substituted enals. Towards this end, we monitored the (*E*)- and (*Z*)-isomer distribution during and after the hydrosilylation of α-benzyl acrolein (**1a**) and (*E*)-hexenal (**2a**) (Figure 2).[27]

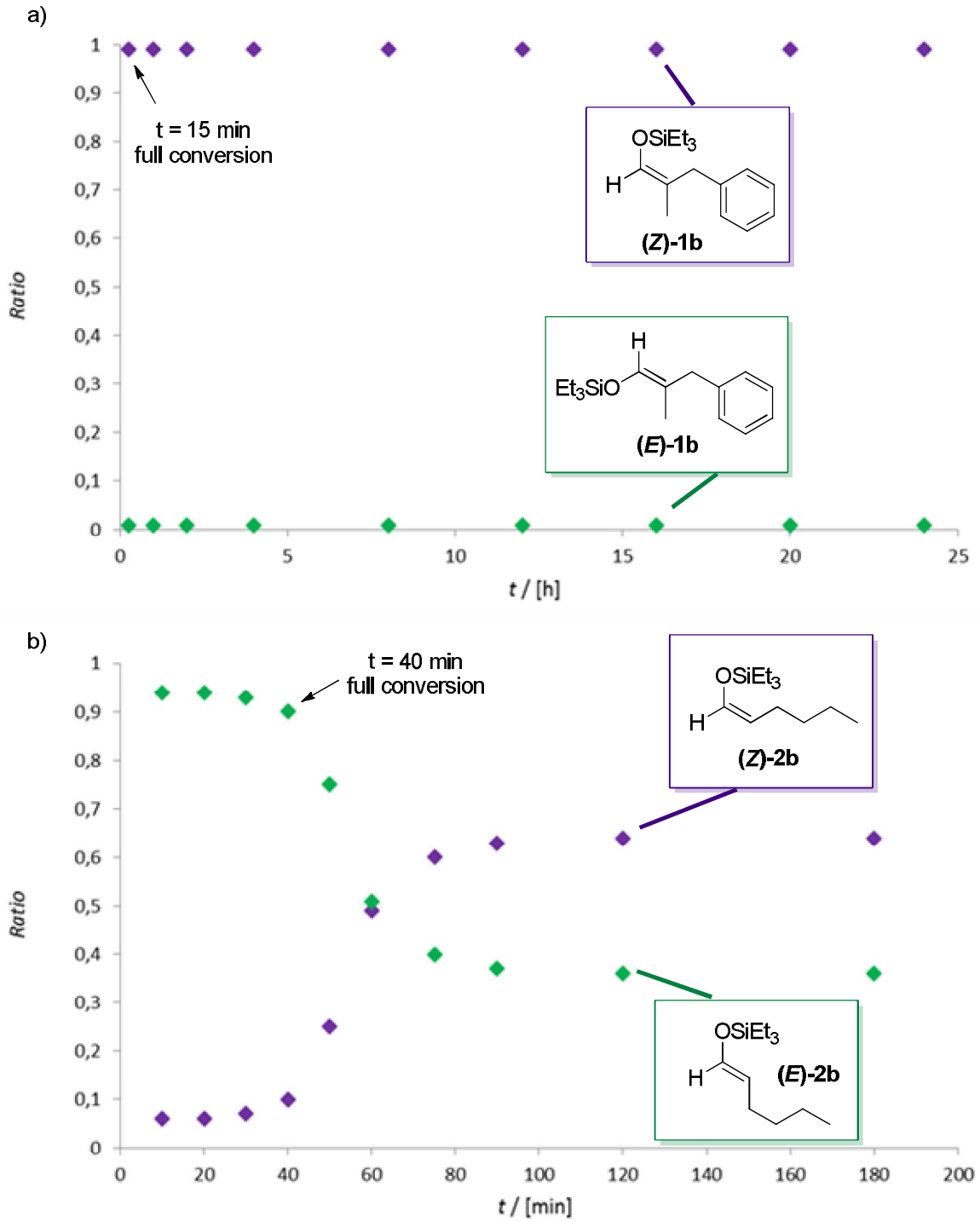


**Figure 2**. Isomer distribution during and after the hydrosilylation reaction. a) With 2-monosubstituted enol silane **1b** and b) with 2,2-disubstituted enol silane **2b**.

The NMR data (Figure 2b) reveals that the stereoselectivity of the hydrosilylation reaction with β-substituted enal **2a** is *Z*:*E* 6:94 (t = 10 min). As the reaction proceeds, the (*E*)-isomer isomerizes slowly to the (*Z*)-isomer during the reaction (*Z*:*E* 7:93, t = 30 min) and at the full conversion (t = 40 min) the isomer ratio is 10:90. Prolonging the reaction time deteriorated the isomer ratio of **2b**.[33] 10 minutes (t = 50 min) after the completion of the reaction, the *Z:E* ratio has decreased to 25:75, and the *Z*:*E* ratio finally stabilizes to 64:36 after 120 min (Figure 2b), a ratio that likely reflects the equilibrium composition under these conditions. In a case of α-substituted enal **1a**, the stereoselectivity of the hydrosilylation reaction was high, *Z*:*E* > 50:1. More precisely, we could no detect the (*E*)-isomer at all in the NMR spectra. In contrast to the product **2b,** we did not observe any isomerization of the product **1b**, even by prolonging the reaction time to 24 hours (Figure 2a).

To assess whether the experimental *Z*:*E* ratios reflect the equilibrium composition, we calculated the solution phase structures of the (*Z*)- and (*E*)-isomers of compounds **1b** and **2b**.[27] Experimentally, the observed isomer ratio for **2b** was 64:36 (*Z*:*E*). The calculated energy difference between **(*Z*)-2b** and **(*E*)-2b** was ΔE = 2.2 kJ/mol, predicting a 71:29 *Z*:*E* isomer ratio for **2b**, in close agreement with the experimental ratio.[27,34] In contrast, in the case of **1b**, the calculated equilibrium isomer ratio (67:33) did not match the experimental ratio (>50:1),[35] suggesting that the stereoselectivity for **(*Z*)-1b** is of kinetic and not of thermodynamic origin.

Isomerization of enol ethers on Pd catalysts is known to take place almost entirely via reversible hydridopalladation, where the hydrogen atom ends up in the β-position of the enol ether on Pd/C.[36] To confirm the fate of a hydrogen atom in the hydrosilylation/isomerization sequence, we carried out a labeling experiment with $Et_3SiD$ and **2a** and allowed the isomerization reaction of **2b** to reach the "thermodynamic equilibrium" (Scheme 4a).[37] As predicted, we observed D-incorporation in the β-position of the enol ether compared to α-position.[27] The proposed reversible mechanism for

the isomerization of **2b** is presented in scheme 4b. In view of the proposed mechanism, a possible reason for the lack of isomerization with 2,2-disubstitued enol silane **1b** (Scheme 4b) is that the rotation of the intermediate $\mathbf{1b^{i}}$ gives a conformation $\mathbf{1b^{ii}}$ in which C-H bond is tilted away from the surface, preventing its interaction with the metal (Scheme 4c). In other words, cleavage of the C-H bond can only occur in a conformation $\mathbf{1b^{i}}$ that leads to same isomer that initially adsorbed on the catalyst (Scheme 4c).

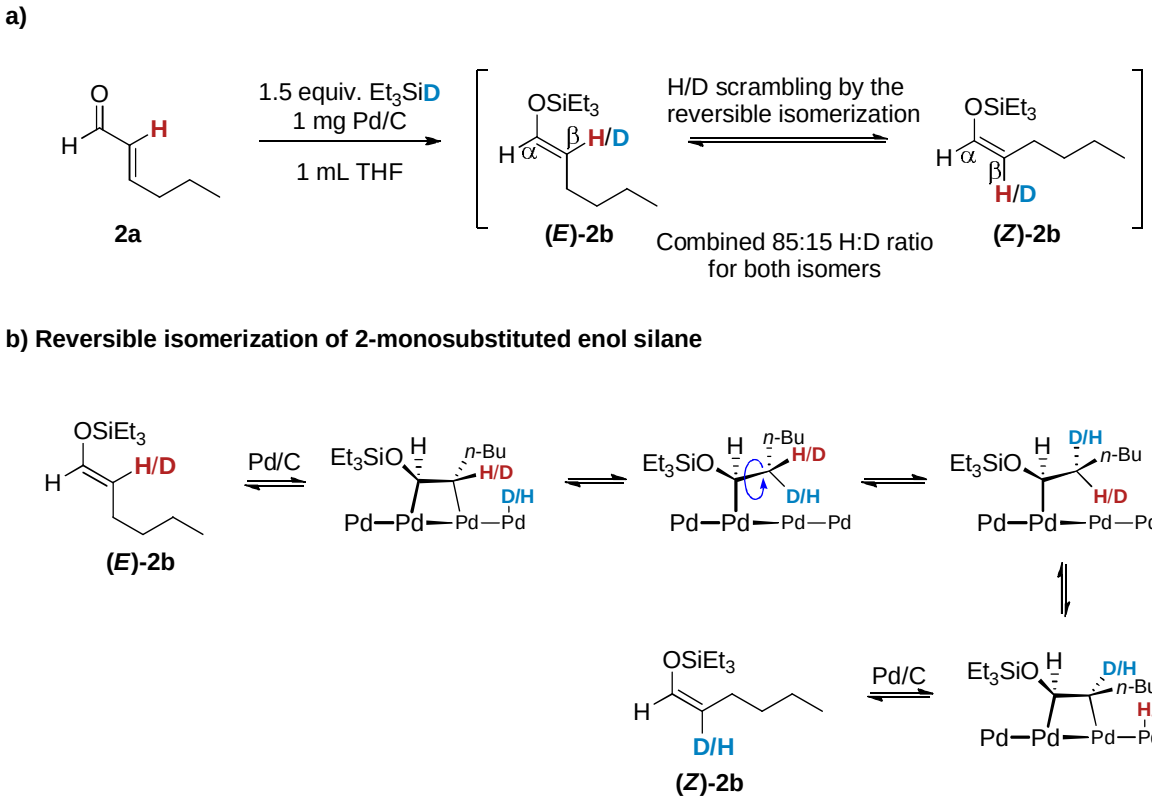


**Scheme 4.** Isomerization of enol silanes: a) labeling experiment with $Et_3SiD$ and **2a**, b) reversible isomerization of 2-monosubstituted enol silane **2b**, c) ineligible isomerization of 2,2-disubstituted enol silane **1b**.

**COMPUTATIONAL STUDIES.** To gain further mechanistic insight into the hydrosilylation reaction, we carried out density functional theory (DFT) calculations for acrolein (**4a**) hydrosilylation with $Me_3SiH$ on Pd(111).[27] Experimentally, enals, such as acrolein (**4a**), are almost

entirely converted to corresponding enol silanes under the optimized reaction conditions.[6,27] However, during the optimization process also allyloxysilanes, saturated aldehydes, and enols, which isomerizes to the saturated aldehyde via keto-enol tautomerism, have been detected.[6,27] According to our recent DFT calculations, acrolein (**4a**) prefers to adsorb from the C=C double bond in the di-σ configuration with the adsorption energy of –55 kJ/mol[5] on Pd(111). We find that $Me_3SiH$ adsorbs dissociatively on Pd(111) with the adsorption energy of –76 kJ/mol. In the optimized geometry, $SiMe_3$ sits on a top position and H at an adjacent/next nearest hollow site.

Scheme 5 summarizes competitive reaction pathways for the hydrosilylation and transfer hydrogenation of acrolein. The hydrosilylation can lead to two isomeric products: enol silane **4b** and allyloxysilane **4f**. According to the calculations, the enol silane is more stable by 28 kJ/mol in the gas phase and by 12 kJ/mol on the Pd(111) surface. Both hydrosilylation products adsorb from the C=C double bond in the di-σ configuration with adsorption energies of –5 (**4b**) and –20 (**4f**) kJ/mol compared to the corresponding species in gas phase. Among the three possible isomeric hydrogenation product molecules (propanal (**4c**), 1-propenol (**4d**) and allyl alcohol (**4e**)), propanal is thermodynamically the most stable molecule in the gas phase by 35 kJ/mol,[38] while their relative stabilities differ on Pd(111). Allyl alcohol and 1-propenol adsorb in the di-σ configuration and their adsorption energies are –49 and –31 kJ/mol with respect to given species in the gas phase. However, propanal (**4c**) prefers to bind to Pd(111) via the carbonyl group in the di-σ configuration with slightly endothermic adsorption energy 1 kJ/mol compared to the gas phase structure.

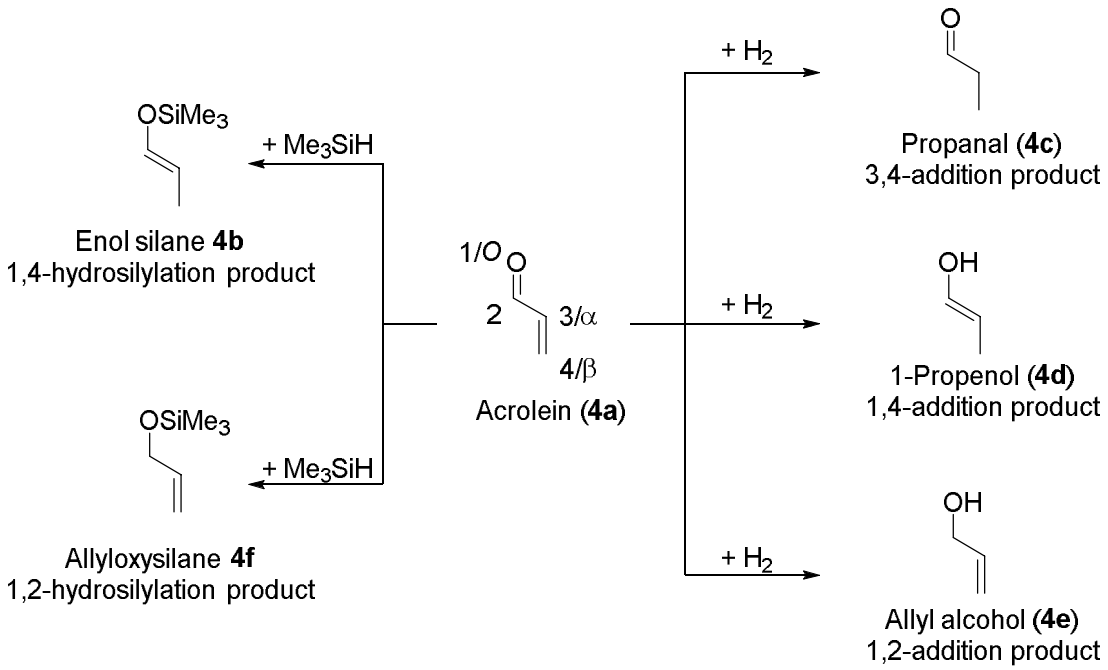


**Scheme 5**. Competitive hydrosilylation and and partial hydrogenation pathways for acrolein (**4a**) to produce hydrosilylation products (enol silane **4b** and allyloxysilane **4f**) and three isomeric hydrogenation products (propanal (**4c**), 1-propenol (**4d**), allyl alcohol (**4e**)).

To computationally determine which of the individual steps hydrogenation or hydrosilylation of acrolein (**4a**) is preferred on Pd(111), we calculated the reaction pathways leading to the products presented in Scheme 5. We have previously studied the hydrogenation of acrolein on a Pd(111) surface (see ref 5). In brief, we found that the formation of propanal (**4c**) and 1-propenol (**4d**) i.e. the 4,3- and 1,4-reductions are energetically more favorable than the 1,2-reduction pathway leading to the ally alcohol (**4e**). Specifically, for 1,2 and 2,1 reductions the low-energy transition states require the ensemble of three or four adjacent metal atoms, which becomes unfeasible at higher surface coverage.

In the hydrosilylation reaction, the enol silane **4b** and the allyloxysilane **4f** can be formed in two different ways: 1) via *O*-silylation, i.e. the formation of an O-Si bond, followed by the H-addition to the 2- or 4-position (1,2- and 1,4-hydrosilylation), or 2) vice versa, with the *O*-silylation taking

place only after the formation of 2- and 4-addition intermediates (2,1- and 4,1-hydrosilylation). In the previous calculations, we found the 2-addition elementary step was found to have the highest barrier among all the H-additions to the acrolein.[5] Hence, the possibility of formation of **4f** via the 2,1-hydrosilylation pathway was rationally excluded. The kinetically most relevant pathways to produce **4b** and **4f** were found to begin with the *O*-silylation (see below, Scheme 6, and the associated discussion) and this process is strongly exothermic. However, the energy differences are small and the 4,1-hydrosilylation pathway presents only 11 kJ/mol higher barrier than the 1,4-hydrosilylation. Consequently, the possibility of a 4,1-addition pathway for the formation of **4b** cannot be ruled out. The *O*-silylation intermediate prefers a $\eta 3\pi(CC)\sigma(C)$ adsorption geometry on Pd(111) (see Section S5.3.1 in the SI). Interestingly, the geometry resembles that of the 1-addition intermediate in acrolein hydrogenation.[5] The comparison of transition state energies shows that the energy difference between the 1,4- and 1,2-hydrosilylation pathways is only 3 kJ/mol favoring the enol silane **4b** formation (See Tables S54 and S55). Experimentally, we did not observe the formation of allyloxysilane **4f** from acrolein (**4a**). Thus, the computed energy difference is far too small to explain observed selectivity. However, this apparent contradiction is readily resolved if the adsorbed silyl species is also included in the computational model (see below).

The kinetically most relevant pathways leading to propanal (**4c**), 1-propenol (**4d**) and enol silane **4b** are summarized in Figure S12.[39] The most striking finding in this figure is that the computational results contradict the experimental results and predict that hydrogenation of acrolein is kinetically more favorable than hydrosilylation: the energy difference between the lowest transition states energies is as large as 64 kJ/mol. However, the steric and electronic effects of the silane were only included in the calculations of the hydrosilylation steps, where both the silyl group and acrolein were simultaneously present in the same unit cell . According to our crossover

experiments (Scheme 2a),[6b] background reactions[30] and experimental precedents,[40] silanes fully dissociate on Pd. To address the extent of coverage of silyl groups on the catalyst under the reaction conditions and the impact of coverage on the transition state geometries and energies of the hydrogenation and hydrosilylation reactions, the adsorption energies were first computed. The computed adsorption energies of $Et_3SiH$ and $Me_3SiH$ (Table S7) and different enals (Table S5) show that the adsorption of silanes onto the Pd(111) surface is stronger than any of the enals. In particular, the adsorption of $Me_3SiH$ is energetically 26 kJ/mol more favorable than the adsorption of acrolein (**4a**). This suggests that there are hydrogen and silyl species adsorbed on the catalyst under the actual reaction conditions and thus high silane coverage probably presents a more realistic model of a Pd catalyst.[41] Therefore, we computed hydrosilylation pathways and the acrolein hydrogenation in the presence of one dissociated MeSiH in the same unit cell at 1/9 ML total coverage.[27] The adsorption energy of the acrolein on the silane pre-covered surface is 55 kJ/mol endothermic at 1/9 ML (**4a$_a$*** in Table S14), while it is –55 kJ/mol on bare Pd(111) at 1/9 ML (**4a*** in Table S5) both energies were calculated with the RPBE functional. The comparison of activation barriers for the *O*-silylation and hydride additions at 1/9 ML silane coverage shows that the hydrosilylation is favored by 38 kJ/mol, which implies that the silane acts both as a reagent and a chemoselectivity modulator.

In our recent DFT study,[5] we demonstrated that selectivity in acrolein hydrogenation depends sensitively on steric effects which can potentially be important here as well. Therefore, we varied the total coverage from 1/9 ML to 1/6 ML and analyzed the impact of steric effects to the kinetically most favored reaction pathways and product selectivity. The presence of dissociated $Me_3SiH$ in the same unit cell with acrolein at 1/9 and 1/6 ML coverage (**4a**), impacts significantly the stereoselectivity of the reaction (see below) via both thermochemistry and kinetics of the

hydrosilylation and hydrogenation steps. A potential energy surface plot for the kinetically most relevant pathways at 1/6 ML coverage on pre-covered Pd surface is shown in Figure 3.[27] The adsorbed silyl group acts as a stereoselectivity modulator, however it does not modify the most stable adsorption geometries of the acrolein, intermediates or products. In general, less space intensive adsorption geometries become energetically more favorable with increasing coverage, similarly to our previous study on the hydrogenation of acrolein.[5]

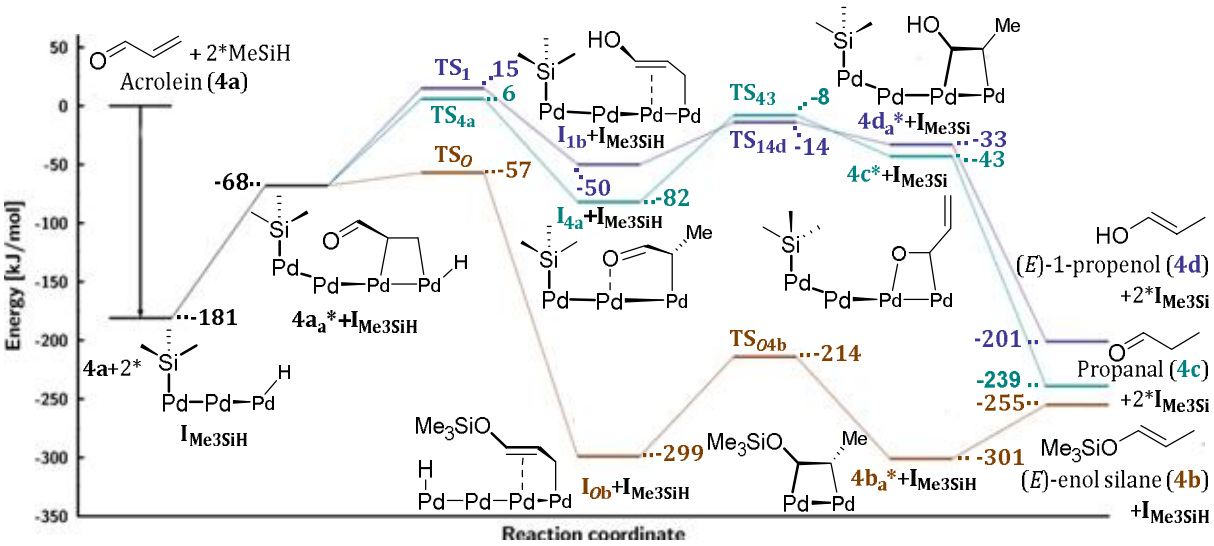


**Figure 3**. PES of the kinetically most relevant pathways for hydrosilylation and for hydrogenation of acrolein **4a** on a Pd(111)-2x3 surface (1/6 ML), calculated with the BEEF-vdW functional.

On the silane pre-covered surface, the *O*-silylation step is nearly spontaneous and the activation energy is only 9 kJ/mol. The reaction is highly exothermic, with the reaction energy of -231 kJ/mol (Scheme 6), which makes desilylation (the reverse process) highly unlikely. We cannot rule out the possibility of a concerted acrolein adsorption and *O*-silylation step but we were unable to identify a transition state for this pathway. The energy difference ($\Delta E_{TS}^{*}$)[42] between the lowest transition state energies leading to *O*-silylated and partially hydrogenated intermediates $\mathbf{I_{Ob}}$ and $\mathbf{I_{4a}}$ is 63 kJ/mol, and clearly demonstrates preference for hydrosilylation over hydrogenation in

agreement with experiments. In addition, the energy difference between $\mathbf{TS}_{O}$ and $\mathbf{TS}_{4a}$ also points out that hydrosilylation prefers the 1,4- pathway to the 4,1- pathway.

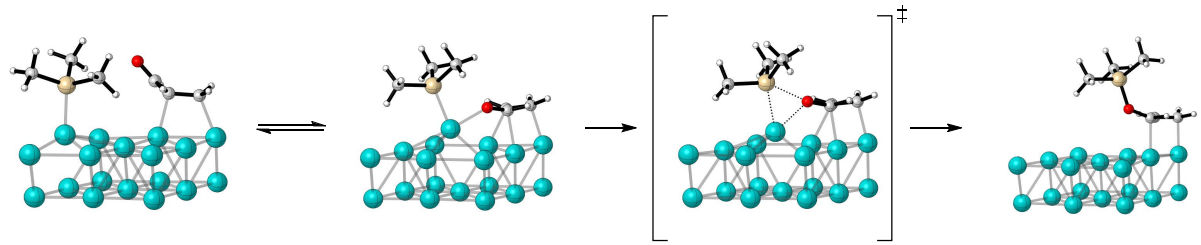


**Scheme 6.** The *O*-silylation elementary step. Relative stabilities are given with respect to the structure $\mathbf{4a_a*}$.

Among the possible intermediates, the *O*-silylated species bind most strongly to Pd(111) and favor a $\eta_3\pi$(CC)σ(C) binding geometry ($\mathbf{I_{Ob}}$). H-addition to the 2-position of an *O*-silylated intermediate (Scheme 5) gives the allyloxysilane **4f**, while the H-addition to the 4-position (Scheme 5) forms the enol silane **4b**. The corresponding activation barriers are 134 and 32 kJ/mol, respectively. Consequently, 1,4-hydrosilylation is favored by 102 kJ/mol over 1,2-hydrosilylation (Figure S14),[43] which nicely agrees with experiments producing only enol silane.[27]

Next, we focused on the stereoselectivity of the hydrosilylation reaction. Hydrosilylation of acrolein (**4a**) can lead to two stereomeric products: (*E*)- and (*Z*)-enol silane **4b,** and possible pathways leading to these two stereomers are summarized in Scheme 7. Experimentally we have observed that the hydrosilylation of acrolein produces (*E*)-enol silane **4b** as a major stereomeric product with the *Z*:*E* ratio equal to 12:88[27] but it is unclear why the (*E*)-isomer dominates.

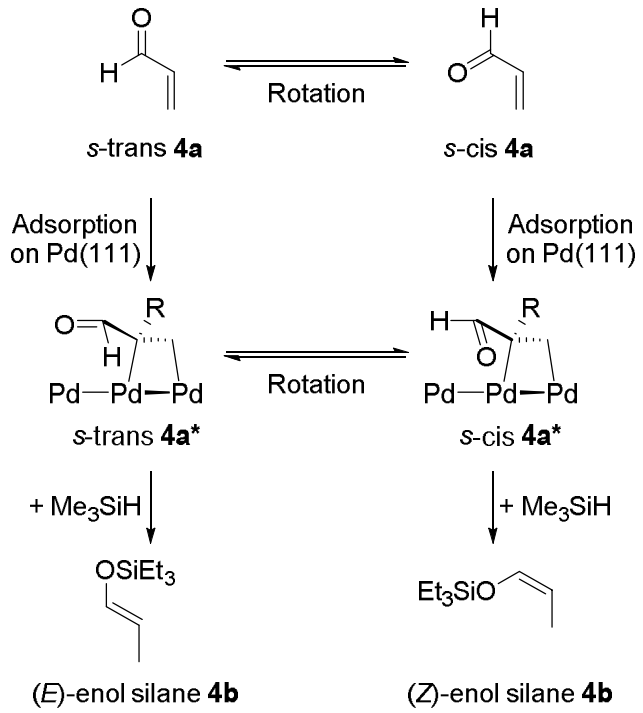


**Scheme 7**. Simplified presentation of different pathways leading to (*E*)- and (*Z*)-enol silane **4b**.

The simple reason could be the adsorption energy difference, and thus we determined the adsorption energies of *s*-trans and *s*-cis conformers of **4a** on Pd(111).[27] However, the difference between the adsorption energies is too small, only 1 kJ/mol, and therefore it does not explain the high stereoselectivities observed in the experiments. As a next step, the reaction pathways were determined from *s*-trans and *s*-cis conformations to (*E*)- and (*Z*)-enol silane **4b** (Figure S12). Again, the energy difference for the reaction barriers of the studied pathways is relatively small ($\Delta E^* = 9$ kJ/mol), and favors the (*Z*)-product pathway.

Finally, the rotation barrier from the *s*-trans conformation of acrolein to a *s*-cis conformation was calculated on the metal surface, and it was found to be 27 kJ/mol higher than the barrier for *O*-silylation (Figure 4).[44] The individual adsorbed acrolein conformers cannot readily equilibrate, as the *O*-silylation step is irreversible, which essentially "freezes" the population of the adsorbed

acrolein conformers. In other words, the Curtin-Hammett principle is not valid for the stereoselectivity of the hydrosilylation reaction, since the reaction barrier is lower than the rotation barrier.[45]

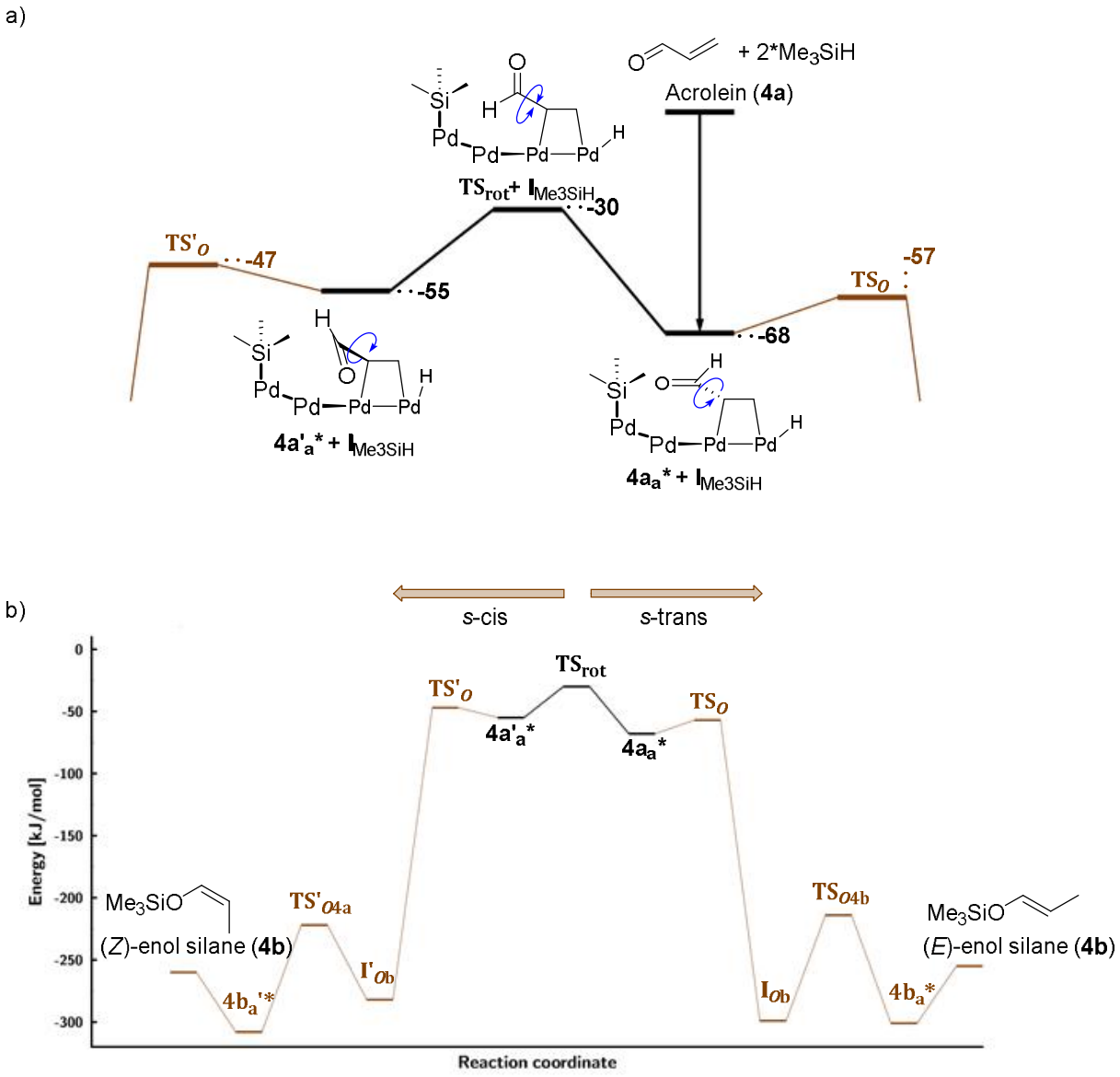


**Figure 4.** Stereoselectivity of the hydrosilylation reaction of acrolein **4a** is not accord with the Curtin-Hammett principle: a) close-up of the *O*-silylation step and b) the complete potential energy surface..

Since the calculations indicate that the hydrosilylation takes place faster than the *s*-trans/*s*-cis interconversion on the surface, we propose that the stereoselectivity of the reaction reflects the *s*-trans/*s*-cis conformer ratio in solution phase. Accordingly, we calculated gas-phase and solution-phase energies of *s*-trans and *s*-cis conformations of several α- and β-substituted enals used in the previous experimental studies.[6,27] These calculations were carried out with the Jaguar package. The equilibrium populations of different conformers were estimated employing Boltzmann distribution at 298.15 K,[46] which nicely explains experimental stereoselectivities given in Tables 1 and 2.[47] Interestingly, similar behavior has been reported for hydrogenation of 1,3-butadiene over a Pd catalyst. In that case, the *Z:E*-ratio of the 1,4-addition products mimics the gas-phase *s*-trans/*s*-cis ratio of 1,3- butadiene.[1c,48] In general, the energy difference between *s*-trans and *s*-cis conformations is larger for α-substituted than for β-substituted enals (Tables 1 and 2). This leads to lower inherent stereoselectivity with β-substituted enals. Together with the isomerization of enol silane products (Figure 2), these effects readily explain the stereoselectivity difference between α- and β-substituted enals.

**Table 1. Gas phase energy difference between *s*-trans and *s*-cis conformations of the *α*-substituted enals and the predicted and obtained isomer ratio of the enol silane products.**

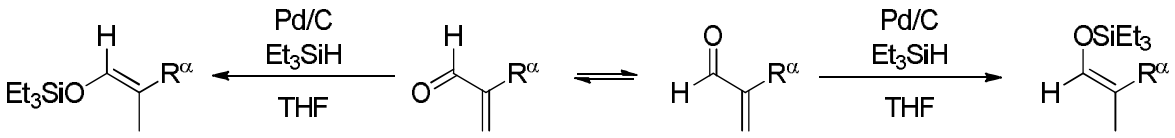


| Entry | Substrate | ΔG = (kJ/mol) *s*-trans – *s*-cis[a] | Predicted stereoselectivity *Z*:*E*[b] | Experimental stereoselectivity *Z*:*E*[c] |
|---|---|---|---|---|
| 1 | 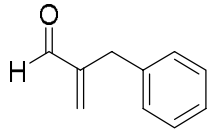 **1a** | -11.1 | 99:1 | >50:1 |

| | | | | |
|---|---|---|---|---|
| 2 | 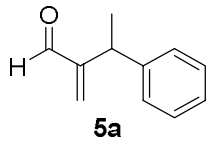 **5a** | -8.3 | 97:3 | >50:1 |
| 3 | 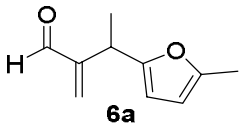 **6a** | -12.1 | 99:1 | 25:1 |
| 4 | 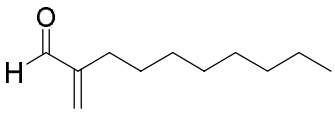 **7a** | -13.3 | 99:1 | >50:1 |
| 5 | 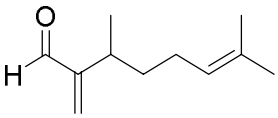 **8a** | -8.0 | 96:4 | >50:1 |

[a] For computational details, see the Supporting Information. [b] The predicted ratio is equal to the ratio of the *s*-cis:*s*-trans conformer populations (based on the most stable conformers for each). See the Supporting Information for details. [c] Isomer ratios after full conversion of the starting material, see ref 6a.

**Table 2. Gas phase energy difference between *s*-trans and *s*-cis conformations of the β -substituted enals and the predicted and obtained isomer ratio of the enol silane products.**

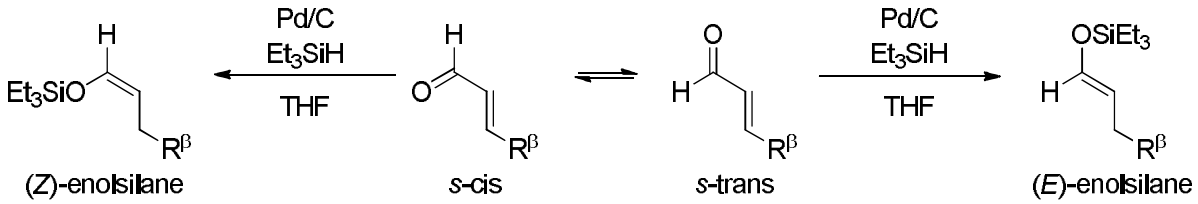


| Entry | Substrate | ΔG = (kJ/mol) *s*-trans – *s*-cis[a] | Predicted stereoselectivity *Z*:*E*[b] | Experimental stereoselectivity *Z*:*E*[c] |
|---|---|---|---|---|
| 1 | 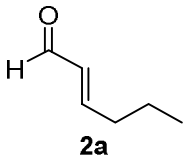 **2a** | -7.7 | 4:96 | 6:94[d] |
| 2 | 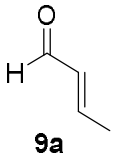 **9a** | -7.4 | 5:95 | 10:90[e] |
| 3 | 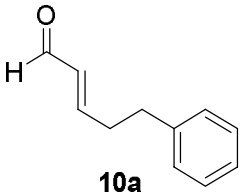 **10a** | -7.2 | 5:95 | 8:92 |
| 4 | 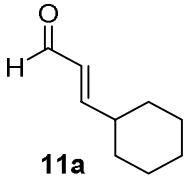 **11a** | -7.9 | 4:96 | 11:89 |
| 5 | 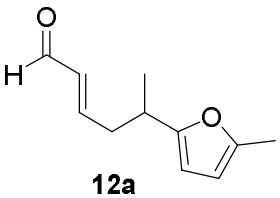 **12a** | -10.0 | 2:98 | 10:90[f] |

[a] For computational details, see the Supporting Information. [b] The predicted ratio is equal to the ratio of the *s*-cis:*s*-trans conformer populations (based on the most stable conformers for each) See the Supporting Information for details. [c] Isomer ratios after full conversion of the starting material, see ref 6a and the Supporting Information. [d] The isomer ratio at 50 % conversion. [e] See the Supporting Information. [f] The isomer ratio at 90 % conversion.

**CONTROL AND OPTIMIZATION EXPERIMENTS.** According to calculations, the *s*-trans and *s*-cis ratio of enals prior to the adsorption step determines stereoselectivity. Thus, the choice of solvent might affect the stereoselectivity of the reaction. Since the dipole moment of *s*-trans conformer is higher than *s*-cis conformer with acrolein (**4a**) and citral (**3a**), we hypothesized that higher *Z*:*E* ratios might be obtained with more polar solvents that could preferentially stabilize the more polar *s*-trans conformer.[49] Citral (**3a**) was chosen as the substrate for the solvent screening, since no post-reaction isomerization was detected in hydrosilylation reactions with citral.[27] The measured *Z:E* ratio varied with the solvent used (Table 3), and indeed, the highest *Z:E* ratios were obtained with polar solvents such as $Et_2O$, THF and EtOAc.[27,50] However, better chemoselectivities were obtained with solvents with a low dielectric constant, such as toluene and $Et_2O$ (Table 3). It should be noted that the chemoselectivity can also reflect the water content in the solvent, as shown in Figures 1c and S9. In summary, $Et_2O$ turned out to be the optimal solvent with regard to chemo- and stereoselectivity.

**Table 3. Chemo- and stereoselectivity of the hydrosilylation of citral (3a) with different solvents.**

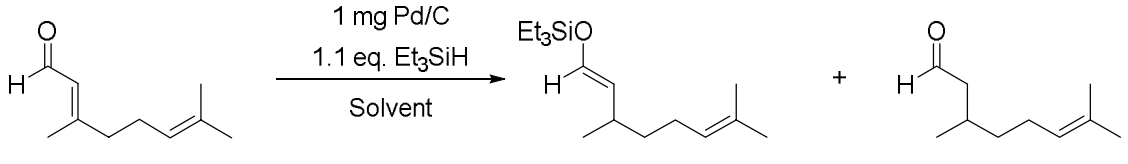


0.30 mmol
**3a** **3b** **3c**

| Entry | Solvent | Dielectric Constants ε | Rxn Time | Conversion % | Product selectivity 3b/3c[a] | *Z*:*E*[a] |
|---|---|---|---|---|---|---|
| 1 | THF | 7.6 | 4 h | 100 % | 8:1 | 1:20 |
| 2 | DCM | 8.9 | 16 h | 75 % | 9:1 | 1:5 |
| 3 | Toluene | 2.4 | 16 h | 92 % | 19:1 | 1:7 |
| 4 | EtOAc[b] | 6.0 | 16 h | 89 % | 7:1 | 1:20 |
| 5 | $Et_2O$ | 4.3 | 16 h | 89 % | 22:1 | 1:20 |

Reaction conditions: **3a** (46 mg, 51 mml, 0.30 mmol, 1.0 eq.), Pd/C (1 mg), triethylsilane (38 mg, 53 mml, 0.33 mmol, 1.1 eq.), solvent (1 mL), room temperature. [a] Determined by $^1$H NMR analysis. [b] EtOAc was dried with $Na_2SO_4$.

In addition, we carried out temperature screening for hydrosilylation of citral (**3a**) to see the effect of temperature variation on the chemo- and stereoselectivity of the reaction (Table S4). In agreement with the literature,[51] the temperature does not have effect on the *s*-trans/*s*-cis ratio of the citral (**3a**), and the stereoselectivity of the hydrosilylation reaction does not change. However, lower temperatures led to poor conversions. For example, only 38 % conversion was reached in 24 h at –20 °C.

With all the information from mechanistic studies at hand, we attempted to improve the chemo- and stereoselectivity for the hydrosilylation of β-substituted acrolein.[52] By carefully excluding all moisture from the reaction mixture, we were able to increase the chemoselectivity of the hydrogenation reaction with citral (**3a**) from 63 % to 90 % isolated yield with *Z*:*E* 1:20 (Scheme

8a). To obtain high stereoselectivity with (*E*)-hexenal (**2a**), we tried to prevent the *E*:*Z*-isomerization by quenching the reaction before the full conversion. When the reaction was quenched at 92 % conversion, the *Z*:*E* ratio increased from 1:9 to 1:19 with 83 % isolated yield (Scheme 8b).

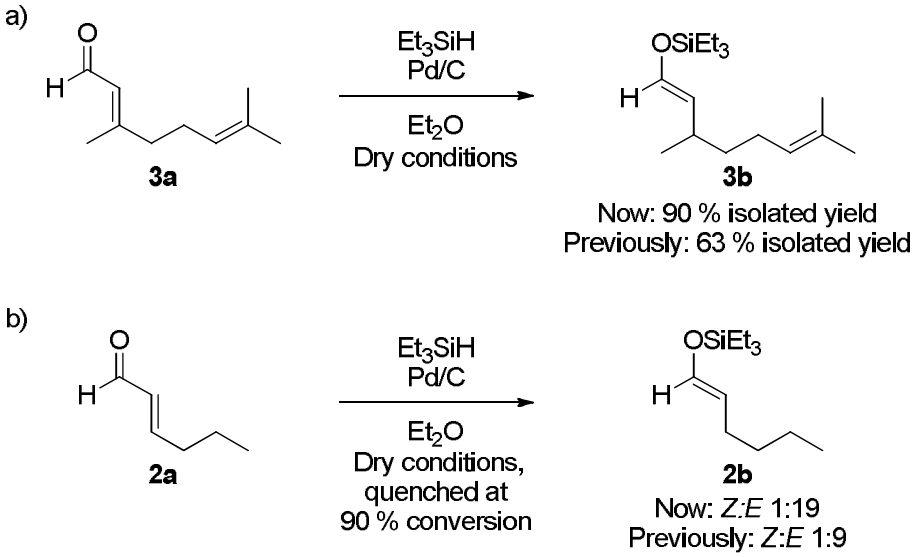


**Scheme 8**. Improved yields and isomer ratios in the hydrosilylation of β-substituted enals: a) Improved yield with citral (**3a**) and b) improved *Z*:*E* ratio with (*E*)-hexenal (**2a**).

## DISCUSSION

**CHEMOSELECTIVITY.** Our previous experimental studies[6] report the formation of saturated aldehyde side product only with the β-substituted but not with the α-substituted enals.[6a] To explain these results, we considered three different mechanistic pathways for the formation of the saturated aldehyde: 1) via hydrolysis of enol silane, 2) via direct hydrogenation of the C=C bond or 3) via transfer hydrogenation mechanism (i.e. via enol intermediate).

The hydrolysis pathway can be ruled out, since enol silanes are stable in presence of water (Scheme 3). Furthermore, a simple hydrogenation mechanism, which herein refers to the hydrogenation of the C=C double bond (3,4-addition), can be excluded as well, as no D-incorporation to the α-position of the side product **3c** was observed in labeling experiments of citral (**3a**). Furthermore, the computed ΔE between hydrogenation and hydrosilylation steps is too high (63 kJ/mol) to explain the formation of the saturated aldehyde via the standard Langmuir–Hinshelwood mechanism.[5] Therefore, the most probable explanation is that the saturated aldehyde most likely forms via a transfer hydrogenation pathway, where the proton comes from the solution phase leading to the enol product, which later tautomerizes to the corresponding saturated aldehyde (Scheme S3).[53] Indeed, we have previously shown that the enol intermediate can be detected experimentally .[29]

The rate of a transfer hydrogenation reaction depends on the water concentration in the reaction mixture (Figure 1). The reason for the observed formation of the saturated aldehyde side-product in the case of β-substituted enals is that even a small amount of water in the reaction mixture is sufficient to promote the transfer hydrogenation mechanism. However, in the case of α-substituted

enals, the rate of hydrosilylation is higher than the rate of transfer hydrogenation even in the presence of small amount of moisture.

In our previous studies, we were able to hydrosilylate enals and cyclic enones but not acyclic enones.[54] The mechanism outlined in this study offers a possible explanation: only sterically unhindered enals and cyclic enones can adopt a flat conformation required for the *O*-silylation step (Scheme 6). In the case of acyclic enones, a methylene or methyl substituent adjacent to the carbonyl group may force it to tilt away from the palladium surface preventing the *O*-silylation step. However, the transfer hydrogenation reaction does not suffer from this limitation, since the proton comes from the solution phase (Scheme S3).

**STEREOSELECTIVITY.** In the previous experiments, we observed a clear trend in the stereoselectivity of the hydrosilylation reaction.[6] The major isomer of the enol silane product corresponds to the *s*-trans conformation of the enal. Based on DFT-calculations, we propose that the Curtin-Hammett principle is not valid for the reaction. The individual adsorbed enal conformers cannot equilibrate from a *s*-trans to a *s*-cis conformer on the Pd surface and the *O*-silylation elementary step is irreversible (Figure 4). The *s*-trans/*s*-cis ratio of the enal in the solution phase determines the stereoselectivity outcome of the hydrosilylation reaction. This is further supported by the computed Boltzmann populations of *s*-trans and *s*-cis enal conformers, which agrees well with the experimental isomer ratio (Tables 1 and 2). In addition, in experiments with citral (**3a**), we observed a small solvent effect in the stereoselectivity of the hydrosilylation reaction (Table 3).

Interestingly, only the 2-substituted enol silanes formed from the β-substituted enals seem to undergo an isomerization after the completed reaction (Figure 2). The isomerization of the 2-

substituted enol silanes in the reaction conditions occurs via reversible hydropalladiation (Scheme 4a). With 2-substituted enol silanes (derived from β-substituted enals) this mechanism leads to *E*:*Z*-isomerization. However, with the 2,2-disubstituted enol silanes (from the α-substituted enals) this mechanism always leads to the same isomer that initially adsorbs to the surface, and isomerization is no longer possible (Scheme 4b).

**MECHANISM.** Scheme 9 presents the complete catalytic cycle of the hydrosilylation reaction on the Pd surface.

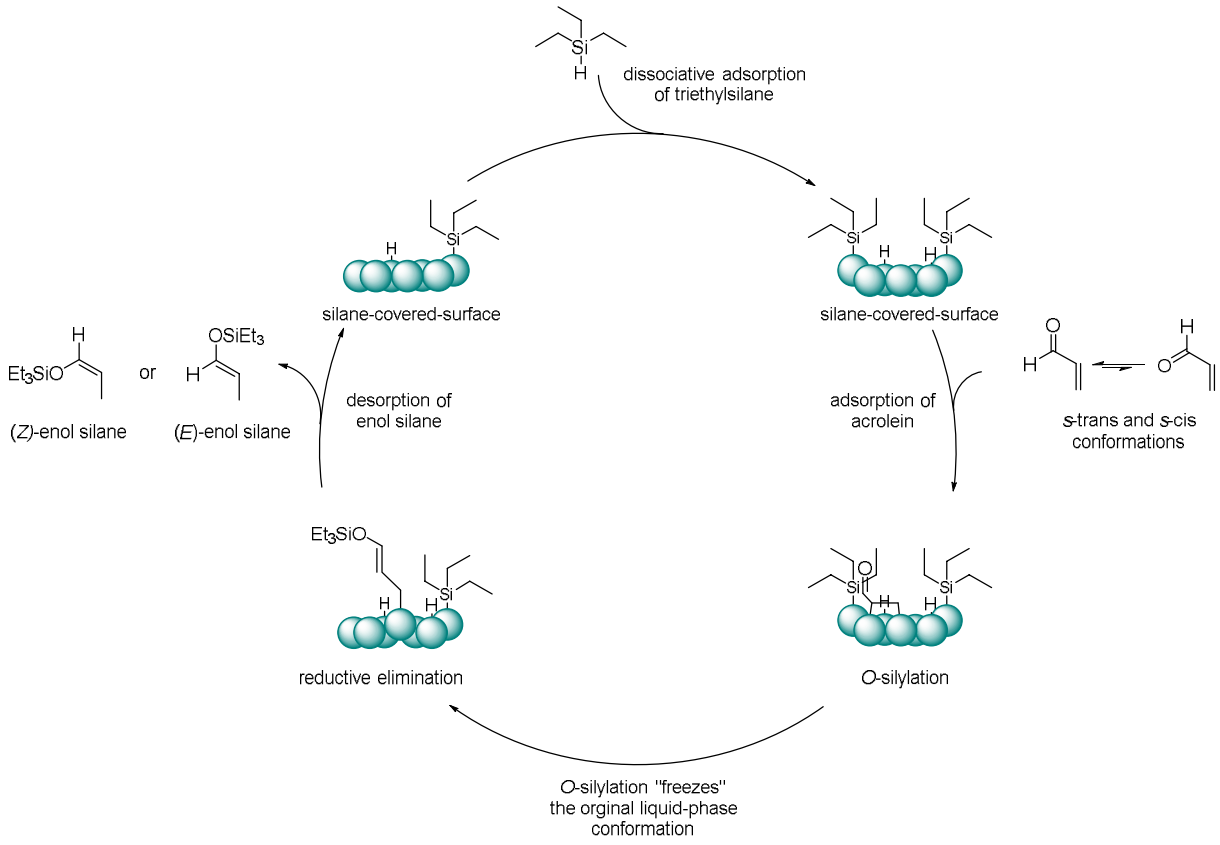


**Scheme 9.** The catalytic cycle of the 1,4-hydrosilylation of enals with triethylsilane and Pd/C.

The catalytic cycle begins with the dissociative adsorption of the triethylsilane onto the Pd-surface. This leads to the high surface coverage of hydrogen atoms and silyl-species. Onto this silane-covered-surface enal adsorbs from the C=C double bond. Before the adsorbed enal can

rotate from a *s*-trans to a *s*-cis conformation or vice versa, it undergoes a rapid irreversible *O*-silylation which "freezes" the original conformer populations. After this, the enol silane desorbs from the surface via the reductive elimination mechanism. The *Z*:*E* ratio of the product is determined by the solution phase ratio of the enal *s*-trans and *s*-cis conformers.

## CONCLUSIONS

In conclusion, we have investigated the mechanism of the heterogeneous Pd-catalyzed hydrosilylation of enals and enones with $Et_3SiH$. The reaction proceeds with good levels of chemo-, region-, and stereoselectivity with stoichiometric amounts of silane and commercial Pd/C catalyst. Experimental and computational results suggest that the hydrosilylation reaction is both thermodynamically and kinetically favored over the competing transfer hydrogenation reaction regime. The transfer hydrogenation, promoted by the presence of water or acid, can also give high chemoselectivity in the presence of other reducible functionalities such as benzyl ethers, nitro groups, or nonconjugated C=C bonds. Experimentally, both hydrosilylation and transfer hydrogenation reactions appear to follow zero-order kinetics on the substrate, suggesting that the catalyst is fully saturated with the substrate. The stereoselectivity of the hydrosilylation with β-substituted enals is compromised by the isomerization of the substrate on the catalyst after the reaction has been completed. Computational investigation of the reaction mechanism with enals indicate that the stereoselectivity of the reaction is due to the rapid *O*-silylation step on the catalyst surface, which "freezes" the original *s*-trans:*s*-cis conformer population of the enal substrate in the solution phase. In addition, we have improved the chemo- and stereoselectivity for the hydrosilylation of β-substituted enals. By excluding all moisture from the reaction mixture, the isolated yield of the hydrogenation of citral (**3a**) to citronellal increased from 63 % to 90 % , and

by quenching the reaction before the full conversion, the stereoselectivity of the hydrosilylation with (*E*)-hexenal (**2a**) increased from 1:9 to 1:19 (*Z*:*E*).

ASSOCIATED CONTENT

**Supporting Information**.

Description of monitoring and screening experiments, as well as additional experiments pertaining to the mechanism, experimental procedures with notes, copies of NMR spectra, potential energy diagrams, computational data, and Cartesian coordinates. This material is available free of charge via the Internet at http://pubs.acs.org.

AUTHOR INFORMATION

**Corresponding Author**

* E-mail: petri.pihko@jyu.fi, karoliina.honkala@jyu.fi

**Author Contributions**

The manuscript was written through contributions of all authors. All authors have given approval to the final version of the manuscript.

**Funding Sources**

Support from the Graduate School of the Faculty of Science, University of Jyväskylä (to S.T.) and a grant from Tekes (2671/31/2013, to K.H. and P.M.P.) are gratefully acknowledged.

ACKNOWLEDGMENTS

We acknowledge the help from M.Sc Juha Siitonen in the deuterium exchange experiments as well as the gas-phase calculations and thank Dr. Elina Kalenius and Ms. Johanna Lind (University of Jyväskylä) for HRMS analyses and Mr. Esa Haapaniemi (University of Jyväskylä)

for assistance with NMR spectroscopy. We also acknowledge access to computational resources provided by the Finnish IT Center for Science (CSC).

REFERENCES

[1] (a) Augustine, R. L. In *Heterogeneous Catalysis for the Synthetic Chemistry*; Marcel Dekker: New York, 1996. (b) Smith, G. V.; Notheisz, F. In *Heterogeneous Catalysis in Organic Chemistry*; Academic Press: New York, 1999. (c) Bartok, M.; Czombos, J.; Felfoldi, K.; Gera, L.; Gondos, G.; Molnar, A.; Notheisz, F.; Palinko, I.; Wittman, G.; Zsigmond, A. G. *Stereochemistry of Heterogeneous Metal Catalysis*; Wiley: New York, 1985.

[2] (a) Guisnet, M.; Barrault, J.; Bouchoule, C.; Duprez, D.; Montassier, C.; Perot, G., Eds. *Heterogeneous Catalysis and Fine Chemicals*; Elsevier: New York, 1988. (b) Guisnet, M.; Barrault, J.; Bouchoule, C.; Duprez, D.; Perot, G.; Maurel, R.; Montassier, C., Eds. *Heterogeneous Catalysis and Fine Chemicals II*; Elsevier: New York, 1991. (c) Guisnet, M.; Barbier, J.; Barrault, J.; Bouchoule, C.; Duprez, D.; Perot, G.; Montassier, C., Eds. *Heterogeneous Catalysis and Fine Chemicals III*; Elsevier: New York, 1993. (d) Blaser, H. U.; Baiker, A.; Prins, R., Eds. *Heterogeneous Catalysis and Fine Chemicals IV*; Elsevier: New York, 1997. (e) Somorjai, G. A.; Kliewer, C. *J. React. Kinet. Catal. Lett*. 2009, *96*, 191–208. (f) Blaser, H.-U.; Malan, C.; Pugin, B.; Spindler, F.; Steiner, H.; Studer, M. *Adv. Synth. Catal*. 2003, *345*, 103– 151.

[3] Zaera, F. *Acc. Chem. Res.,* 2009, *42*, 1152–1160.

[4] (a) Gokhale, A. A.; Dumesic, J. A.; Mavrikakis, M. *J. Am. Chem. Soc.,* 2008, *130*, 1402–1414. (b) Plata, J. J.; García-Mota, M.; Braga, A. A. C.; López, N.; Maseras, F. *J. Phys. Chem. A* 2009, *113*, 11758–11762. (c) Zope, B. N.; Hibbitts, D. D.; Neurock M.; Davis, R. J. *Science,* 2010, *330*, 74–78. (d) García-Melchor, M.; Bellarosa, L.; López, N. *ACS Catal.* 2014, *4*, 4015–4020. (e) Luo, J.; Yun, H.; Mironenko, A. V.; Goulas, K.; Lee, J. D.; Monai, M.; Wang, C.; Vorotnikov, V.; Murray, C. B.; Vlachos, D. G.; Fornasiero, P.; Gorte, R. J. *ACS Catal.* 2016, *6*, 4095–4104.

[5] Tuokko, S.; Pihko, P. M.; Honkala, K. *Angew. Chem. Int. Ed.* 2016, *55*, 1670–1674.

[6] (a) Tuokko, S.; Pihko, P. M. *Org. Process. Res. Dev*. 2014, *18*, 1740. (b) Benohoud, M.; Tuokko, S.; Pihko, P. M. *Chem. Eur. J*. 2011, *17*, 8404–8413.

[7] (a) Mukaiyama, T. In *Organic Reactions*; Wiley: New York, 1982; Vol. 28, p 203. (b) Denmark, S. E.; Bui, T. *J. Org. Chem*. 2005, *70*, 10190–10193. (c) Boxer, M. B.; Yamamoto, H. *J. Am. Chem. Soc*. 2007, *129*, 2762–2763.

[8] For an example, see: Duffy, J. L.; Yoon, T. P.; Evans, D. A. *Tetrahedron Lett.* 1995, *51*, 9245-9248.

[9] For a general reviews of conjugate reduction, see: (a) Mayes, P. A.; Perlmutter, P. In *Modern Reduction Methods*; Andersson, P. G., Munslow, I. J., Eds.; Wiley-VCH: New York, 2008; pp 87–106. (b) Keinan, E.; Greenspoon, N. In *Comprehensive Organic Synthesis*; Trost, B. M., Fleming, I., Eds.; Pergamon Press: Oxford, 1991; pp 553–557.

[10] (a) Herath, A.; Montgomery, J. *J. Am. Chem. Soc*. 2008, *130*, 9132– 8133. (b) Sumide, Y.; Yorimitsu, H.; Oshima, K. *J. Org. Chem*. 2009, *74*, 7986–7989.

[11] For a review, see: (a) Deutsch, C.; Krause, N.; Lipshutz, B. H. *Chem. Rev*. 2008, *108*, 2916–2927. For selected procedures involving copper catalysis, see: (b) Mahoney, W. S.; Brestensky, D. M.; Stryker, J. M. *J. Am. Chem. Soc*. 1988, *110*, 291–293. For enantioselective conjugate reduction: (c) Appella, D. H.; Moritani, Y.; Shintani, R.; Ferreira, E. M.; Buchwald, S. L. *J. Am. Chem. Soc*. 1999, *121*, 9473– 9474. (d) Hughes, G.; Kimura, M.; Buchwald, S. L. *J. Am. Chem. Soc*. 2003, *125*, 11253–11258.

[12] (a) Keinan, E.; Greenspoon, N. *J. Am. Chem. Soc*. 1986, *108*, 7314–7325. For an enantioselective conjugate reduction, see: (b) Tsuchiya, Y.; Hamashima, Y.; Sodeoka, M. *Org. Lett*. 2006, *8*, 4851–4854. (c) Monguchi, D.; Beemelmanns, C.; Hashizume, D.; Hamashima, Y.; Sodeoka, M. *J. Organomet. Chem*. 2008, *693*, 867–873.

[13] (a) Ojima, I.; Kogure, T.; Nagai, Y. *Tetrahedron Lett*. 1972, *13*, 5035–5038. (b) Evans, D. A.; Fu, G. C. *J. Org. Chem*. 1990, *55*, 5678– 5680. For an enantioselective conjugate reduction: (c) Kanazawa, Y.; Nishiyama, H. *Synlett* 2006, 3343–3345.

[14] Iron: (a) Collman, J. P.; Finke, R. G.; Matlock, P. L.; Wahren, R.; Komoto, R. G.; Brauman, J. I. *J. Am. Chem. Soc*. 1978, *100*, 1119−1140. Molybdenum: (b) Keinan, E.; Perez, D. *J. Org. Chem*. 1987, *52*, 2576−2580. Tin: (c) Hays, D. S.; Scholl, M.; Fu, G. C. *J. Org. Chem*. 1996, *61*, 6751−6752. Manganese: (d) Magnus, P.; Waring, M. J.; Scott, D. A. *Tetrahedron Lett*. 2000, *41*, 9731−9733. Titanium: (e) Kosal, A. D.; Ashfeld, B. L. *Org. Lett*. 2010, *12*, 44−47. Gold and Palladium alloy: (f) Chen, Q.; Tanaka, S.; Fujita, T.; Chen, L.; Minato, T.; Ishikawa, Y.; Chen, M.; Asao, N.; Yamamoto, Y.; Jin, T. *Chem. Commun*. 2014, *50*, 3344–3346.

[15] (a) Leping, L.; Lin, S.-C.; Fukuyama, T. *J. Am. Chem. Soc.* 1990, *112*, 7050– 7051, (b) Tokuyama, H.; Fukuyama, T. *Aldrichim. Acta* 2004, *37*, 87– 96.

[16] Graham, T. H.; Liu, W.; Shen, D.-M. *Org. Lett.* 2011, *13*, 6232– 6235.

[17] Enkovaara, J.; Rostgaard, C.; Mortensen, J. J.; Chen, J.; Dulak, M.; Ferrighi, L.; Gavnholt, J.; Glinsvad, C.; Haikola, V.; Hansen, H. A.; Kristoffersen, H. H.; Kuisma, M.; Larsen, A. H.; Lehtovaara, L.; Ljungberg, M.; Lopez-Acevedo, O.; Moses, P. G.; Ojanen, J.; Olsen, T.; Petzold, V.; Romero, N. A.; Stausholm-Møller, J.; Strange, M.; Tritsaris, G. A.; Vanin, M.; Walter, M.; Hammer, B.; Häkkinen, H.; Madsen, G. K. H.; Nieminen, R. M.; Nørskov, J. K.; Puska, M.; Rantala, T. T.; Schiøtz, J.; Thygesen, K. S.; Jacobsen, K. W. *J. Phys.: Condens. Matter.,* 2010, *22*, 253202.

[18] https://wiki.fysik.dtu.dk/gpaw

[19] Blöchl, P. E. *Phys. Rev. B.: Condens. Matter,* 1994, *50*, 17953.

[20] Perdew, J. P.; Burke, K.; Ernzerhof, M. *Phys. Rev. Lett.,* 1996, *77*, 2865.

[21] Wellendorff, J.; Lundgaard, K. T.; Møgelhøj, A.; Petzold, V.; Landis, D. D.; Nørskov, J. K.; Bligaard, T.; Jacobsen, K. W. *Phys. Rev. B.,* 2012, *85*, 235149.

[22] (a) Jaguar, version 8.8, Schrödinger, LLC, New York, NY, 2009. (b) Maestro, version 10.2.010, Schrödinger, LLC, New York, NY, 2009.

[23] (a) The M06-2X functional is described in Zhao, Y.; Truhlar, D.G. *Theor. Chem. Acc*. 2008, *120*, 215-241. It was chosen due to its superior performance in the conformational analysis of silyl-containing organic molecules, see: (b) Bjornsson, R.; Arnason, I. *Phys. Chem. Chem. Phys*., 2009, *11*, 8689–8697. (c) Walker, M.; Harvey, A. J. A.; Sen, A.; Dessent, C. E. H. *J. Phys. Chem. A*, 2013, *117*, 12590–12600.

[24] (a) For the average particle size in the crossover experiment see: reference 6b. (b) For the average particle size in commercial Pd/C see: Duplais, C.; Forman, A. J.; Baker, B. A.; Lipshutz, B. H. Chem. Eur. J. 2010, 16, 3366–3371.

[25] Conrad, H.; Ertl, G.; Latta, E. E. *Surf. Sci.,* 1974, *41*, 435–446.

[26] For complete monitoring experiments and the transfer hydrogenation in presence of $H_2SO_4$, see the Supporting Information.

[27] For more details, see the Supporting Information.

[28] Despite a careful drying, Pd/C still carries water to the reaction mixture, see tables S1 and S2 in the Supporting Information.

[29] In the transfer hydrogenation conditions an enol intermediate is observed during the reaction, see ref 30.

[30] Tuokko, S.; Pihko, P. M. *Synlett*, 2016, *27*, 1649–1652.

[31] See also transfer hydrogenation of 1a with $H_2SO_4$ in figure S5.

[32] In the previous experiments, the highest amount of saturated aldehyde side-product (18 %) was observed with citral (3a). As a result, 3a was a convenient substrate for the labeling experiment.

[33] Isomerization after the completion of the reaction is also observed with other β-substituted enals, see ref 6a.

[34] McQuarrie D. A.; Simon, J. D. In *Physical Chemistry: a molecular approach*, University Science Books, 1997.

[35] Experimentally the observed isomer ratio for 1b was *Z*:*E* > 50:1. The calculated energy difference (ΔE = 1.0 kJ/mol) predicts 60:40 *Z*:*E* isomer ratio. For more details, see the Supporting Information.

[36] Yu, J.; Spencer, J. B. *Chem. Commun.,* 1998, 1103.

[37] Excess (1.5 equiv) of $Et_3SiD$ was used in the reaction conditions. For more details, see the Supporting Information.

[38] Kliewer, C. J.; Bieri, M.; Somorjai, G. A. *J. Am. Chem. Soc*. 2009, *131*, 9958–9966.

[39] For the hydrogenation of acrolein 4a on Pd(111) surface we used data from our previously published article: ref 5.

[40] (a) Shimizu, K.; Kubo, T.; Satsuma, A. *Chem.–Eur. J.* 2012, *18*, 2226–2229. (b) Mitsudome, T.; Noujima, A.; Mizugaki, T.; Jitsukawa, K.; Kaneda, K. *Chem. Commun*. 2009, 5302–5304. (c) Mitsudome, T.; Arita, S.; Mori, H.; Mizugaki, T.; Jitsukawa, K.; Kaneda, K. *Angew. Chem., Int. Ed*. 2008, *47*, 7938–7940. (d) John, J.; Gravel, E.; Hagege, A.; Li, H.; Gacoin, T.; Doris, E. *Angew. Chem., Int. Ed*. 2011, *50*, 7533–7536. (e) Jeon, M.; Han, J.; Park, J. *ChemCatChem* 2012, *4*, 521–524. (f) Jeon, M.; Han, J.; Park, J. *ACS Catal*. 2012, *2*, 1539–1549. Theoretical studies: Kamachi, T.; Shimizu, K-I.; Yoshihiro, D.; Igawa, K.; Tomooka, K.; Yoshizawa, K. *J. Phys. Chem. C* 2013, *117*, 22967–22973.

[41] For more details of the dissociation of trimethylsilane on Pd(111) surface, see the Supporting Information Section 5.5.1.1.

[42] Calculated as the difference of the transition state energies: $E\_TS_{O\text{-silylation}} - E\_TS_{4b}$.

[43] An extra silyl-group was placed into the unit cell. Note that, during the reaction more silyl should always be accessible to adsorb on the Pd-surface as in the experiments excess of $Et_3SiH$ is used. For more details, see the Supporting Information.

[44] The rotation barrier on the Pd-surface increases with more bulky enals, see Table S6.

[45] A. D. McNaught, A. Wilkinson in IUPAC Compendium of Chemical Terminology, 2nd ed. (the "Gold Book"), Blackwell Scientific Publications, Oxford, 1997; XML on-line corrected version: http://goldbook.iupac.org (2006-), created by M. Nic, J. Jirat, B. Kosata, updates compiled by A. Jenkins.

[46] McQuarrie D. A.; Simon, J. D. In *Physical Chemistry: a molecular approach*, University Science Books, 1997.

[47] The gas phase and solution phase energies correspond to the lowest energy conformers. For (*E*)-hexenal (2a), a more thorough conformer population analysis, including both antiperiplanar (app) as well as gauche conformers, indicated that taking into account the alternative higher energy conformers does not significantly alter the *s*-trans:*s*-cis ratio. See the Supporting Information for further details.

[48] Meyer, E. F.; Burwell, R. L., Jr, *J. Am. Chem Soc.*, 1963, *85*, 2881–2887.

[49] For dipole moment of acrolein, see: (a) Blom, C. E.; Grassi, G.; Bauder, A. *J. Am. Chem. Soc.* 1984, *106*, 7427–7431. For dipole moment of citral, see: (b) Chen, C.-Y.; Le Fèvre, R. J. W. *J. Chem. Soc*. 1965, 5528–5533.

[50] The solvent effect to the stereoselectivity of the hydrosilylation α-substituted enals is modest, see ref 6a.

[51] Pihlasalo, J.; Klika, K.D.; Murzin, D. Yu.; Nieminen, V. *J. Mol. Struct. (THEOCHEM)*, 2007, *814*, 33–41.

[52] The hydrosilylation reaction with α-substituted enals almost uniformly gives enol silanes as a product with high steroselectivities (*Z*:*E* > 50:1).

[53] See proposed catalytic cycle in the Supporting Information section 2.4.

[54] The cyclic enones i.e. cyclohexenone and carvone can undergo the hydrosilylation reaction, see ref 6a.

Insert Table of Contents Graphic and Synopsis Here